Research Article Vol. 57, No. 10 / 1 April 2018 / Applied Optics 2727

applied optics

Dual-plane slightly off-axis digital holography based on a single cube beam splitter

Miguel León-Rodríguez,[1,*] Juan A. Rayas,[2,3] Raúl R. Cordero,[3] Amalia Martínez-García,[2] Adrián Martínez-Gonzalez,[4] Alejandro Téllez-Quiñones,[5] Pedro Yañez-Contreras,[1] and Orlando Medina-Cázares[1]

[1]Universidad Politécnica de Guanajuato, Av. Universidad sur 1001, C.P. 38496 Cortázar, Guanajuato, Mexico
[2]Centro de Investigaciones en Óptica, A.C. Loma del Bosque 115, C.P. 37150 Leó, Guanajuato, Mexico
[3]Universidad de Santiago de Chile, Casilla 307 Correo 2, Santiago, Chile
[4]Universidad Politécnica del Bicentenario, Silao-Romita Km 2, C.P. 36283 Silao de la Victoria, Guanajuato, Mexico
[5]CONACYT-Centro de Investigación en Ciencias de Información Geoespacial, Carr. Sierra Papacal-Chuburna Km. 5, C.P. 97302 Mérida-Yucatán, Mexico
*Corresponding author: y_migue@hotmail.com

Received 28 November 2017; revised 20 February 2018; accepted 22 February 2018; posted 27 February 2018 (Doc. ID 314462); published 30 March 2018

In order to recover the holographic object information, a method based on the recording of two digital holograms, not only at different planes but also in a slightly off-axis scheme, is presented. By introducing a π-phase shift in the reference wave, the zero-order diffracted term and the twin image are removed in the frequency domain during the processing of the recorded holograms. We show that the zero-order elimination by the phase-shifted holograms is better than working with weak-order beam and average intensity removal methods. For recording experimentally two π-shifted holograms at different planes slightly off-axis, a single cube beam splitter is used. Computer simulations and experimental results, carried out to validate our proposal, show a high accuracy of $\pi/14$ that can be comparable with phase-shifting digital holography. For high fringe spacing, our proposal could be applied in electron holography, avoiding high voltage in a biprism.

OCIS codes: (170.0110) Imaging systems; (170.3010) Image reconstruction techniques; (170.3660) Light propagation in tissues; (090.1995) Digital holography; (100.5070) Phase retrieval.

https://doi.org/10.1364/AO.57.002727

1. INTRODUCTION

The analysis in the transmission and the optical thickness of an object in a short period of time is crucial in many fields of imaging research. In addition, a non-invasive method is desired to perform the test. For phase images with sub-wavelength accuracy along the axial direction, digital holography (DH) has become a novel tool in the study of samples that mainly yield quantitative information of the transmitted-or-reflected wavefront through three-dimensional (3D) objects. This non-invasive method is based on the acquisition of an hologram formed by an object wave that interferes with a reference wave [1,2]. The complex amplitude of the object is recovered when the hologram is re-illuminated by a digital replica of the reference wave, which allows us to have quantitative measurements of phase and amplitude images of the specimen [3]. Due to the availability of the modern high-resolution image sensors, DH is applied on diverse fields of knowledge, where fine phase measurement is required. Some of those applications include the analysis and characterization of micro-electromechanical (MEM) and micro-opto-electromechanical systems (MOEMs) [4–7], the study of biological samples [8–11], and the measurement of capillarity waves in micro-fluids [12], where the reconstruction distance, a unique characteristic of DH, plays an important role. However, when the hologram is recorded, a potentially disturbing "twin image" and a non-diffracted (DC term) of the object wave appear in addition to the original object.

In DH, a digital hologram can be obtained from either off-axis [10,13,14] or on-line [15] optical configurations; the difference lies in the interference angle between a reference wave and the object wave. In an off-axis configuration, the interference angle is within a particular range of a few degrees, defined by the resolution of the CCD [16]. The reconstruction of this hologram results in the real image separated from the undiffracted part of the reconstruction wave (or DC term) and the so-called "twin image" (or virtual image). To eliminate the DC term and the virtual image, a filtering frequency method is applied. As a result, the wavefront of the object is recovered [17]. Because a single hologram is enough for

numerical reconstruction of the object wavefront, this configuration is suitable in the image acquisition of dynamic processes. However, because of the interference angle, this configuration does not make efficient use of the available space-bandwidth of the detector; thus, higher spatial frequency components of the object information might be lost [16], and, hence, from an imaging point of view, the lateral resolution of the reconstructed image is decreased. In an in-line configuration, the interference angle is set to 0 deg. The reconstruction of this hologram results from the superimposition of the real image with the DC term and the virtual image. Indeed, an in-line configuration is more accurate than the off-axis counterpart is. However, many images are required to eliminate the DC term and the virtual components. For example, Yamaguchi and Zhang applied the phase-shifting technique, which needs at least three in-line digital holograms to reconstruct the object wave [18]. Gabor holography, trough iterative algorithms, presents an alternative to attain the object wave. Depending on the application, a variety of different constraints can be introduced, although it is not possible, in general, to find a method that guarantees convergence to the true solution [19]. It often happens that the algorithm gets "trapped" in local error-minima and ends up with an imprecise approximation of the original object. Zang *et al.* described an in-line reconstruction method using two axially displaced intensity measurements and verified it with numerical simulations using amplitude objects [20]. In this method, a weak object beam is assumed to remove the zero-order image; meanwhile, the twin image is eliminated by an algebraic manipulation in the Fourier domain. This assumption requires that the object wave should be weak in comparison to the reference, making it sensitive to noise as Situ *et al.* mentioned [21]. As an alternative to eliminate the zero-order image, Situ proposed a π-shifting in the reference phase. However, the scheme still requires four recorded holograms for reconstruction purposes with two steps (0 and π) of phase-shifting in the reference beam. Thus, from the point of view of the number of measurements, the method does not provide much advantage for classical phase-shifting methods as Das *et al.* commented [22]. In 2010, Ryle *et al.* used a dual-wavelength in-line configuration that satisfied Fresnel equivalency between the wavelength and the reconstruction distance and the Laplacian approximation, but they present results over amplitude objects only [23]. Recently, Das *et al.* [22] presented an extension of this method for both amplitude and phase object information, whereas Wang *et al.* [24] used a liquid crystal modulator to perform the double plane approach at 0.05 mm from other recording planes. To suppress the zero-order diffracted wave, while keeping the object and the reference beam amplitudes comparable, they performed the method of subtraction of average intensity of the entire hologram (SAI). The twin image is eliminated by an algebraic manipulation in the Fourier domain. In these dual-plane methods, commented on above, a plane wave and on-axis configuration should be required. The better method to suppress the DC term is that presented by Situ *et al.* [21], where a phase-shifting dual-plane (PSDP) in the reference beam is performed. This is because the subtracted term is precisely the object diffraction distribution.

In this paper, we extend the dual-plane in-line DH concept, showing its feasibility to perform at a slightly off-axis scheme for first time, to the best of our knowledge. To suppress the zero-order diffracted wave, we employ 0 and π of phase-shifting in the reference beam; this is the PSDP. Numerical and experimental evaluations show that the PSDP method delivers results that are more accurate than SAI and weak object beam methods, not only in amplitude distribution but also in phase distribution. A single cube beam-splitter (SCBS) is used for recording the shifted digital holograms at each plane. With this interferometer, only two records are necessary to avoid environment fluctuations, calibration errors in phase-shifting, and system fluctuations. The theoretical evaluation, computer simulation, and experimental results validate our proposal. The results are obtained using a phase-amplitude object and are compared with the well-known phase-shifting DH technique. As we know, this configuration with this interferometer has not been used in DH, as we present in this paper. Additionally, it is worth noting that only dual-plane DH has been used in the in-line configuration, but we extend the dual-plane DH method to the slightly off-axis scheme. This gives us some degree for the misalignment of the optical setup and the possibility to use SCBS. We believed that this proposal would be useful in DH microscopic. This method can be applied in electron holography (EH) in order to get a larger zone of overlap width, lower interference fringe spacing, and good contrast of the interferometric fringes.

2. METHOD

The principle is outlined in Fig. 1. The optical setup is based on a Gates' interferometer configuration [25], whose basic components are a laser beam source and a commercial non-polarizing cube beam splitter (BS) 50T–50R. As depicted in Fig. 1(b), two π-shifted interference patterns are obtained simultaneously, where one of them is the reflection of the other and vice versa.

This BS is composed of two right angle prisms cemented together by their large faces; one of the prisms' faces is precisely deposited on the thin film that generates the beam splitting [see Fig. 2(a)]. Phase shifts are induced according to the theory involved with Fresnel equations for wavefront reflections and

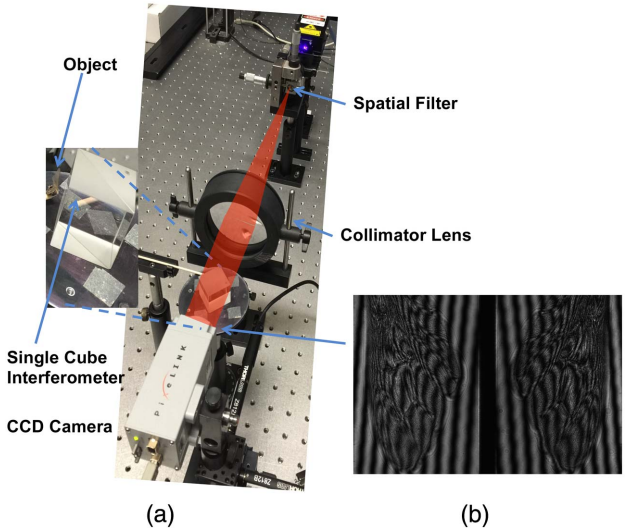

Fig. 1. Single cube interferometer; (a) zoom into target and (b) two π–shifted holograms next to each other.

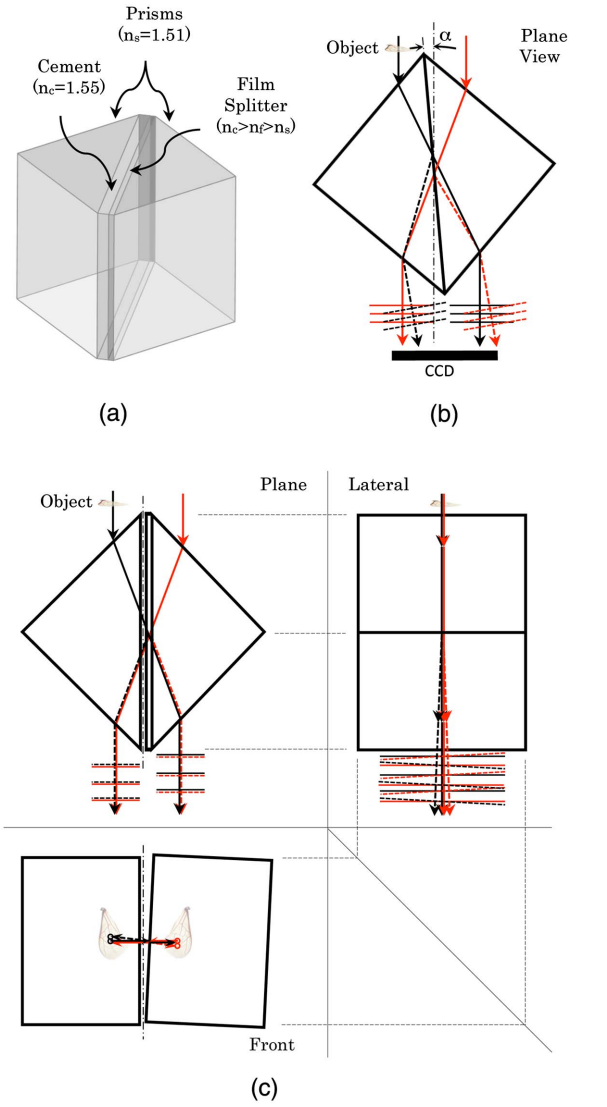

Fig. 2. (a) Single cube beam splitter, (b) top view of ray tracing for the interferometric configuration used in this work showing the effect of the cube beam-splitter rotation, and (c) lateral and front views of ray tracing for the interferometric configuration used in this work showing the effect of the imperfect parallelism cube beam splitter.

transmissions through dielectric media. A π-phase-shift is generated when the wave is reflected from a low to a high refractive index media. If the thin film is dielectric and its refractive index has a value n_f between n_s, the refractive index for the glass, and n_c, the corresponding for the adhesive, then a π-phase-shift is induced at the output of the interferometer [see Fig. 2(a)] [26]. The beam from the laser source is expanded and collimated in order to attain a unit plane wave. As shown in Fig. 1, the expanded and collimated laser beam is impinged on the edge of the splitter cube parallel to the junction of the prisms that are symmetrically illuminated. In order to differentiate the portion of the beam impinging on each prism, black and red lines [ray traces in Fig. 2(b)] are drawn in the interferometric schema. Once the first refraction takes place with no phase changes induced, the beam is split into two contributions, reflection and transmission, respectively. When the beam leaves the cube, the refraction happens again. The same phenomenon takes place in the other side (black line) with a phase change. At the output of each prism there are two interference patterns π-shifted to each other, whose fringe pattern frequency can be increased (off-axis configuration) by turning (twist) the BS cube [depicted in Fig. 2(b)]. The waves related in this interference are called the reference R and the object O. In addition, to get the so-called slightly off-axis geometry, an α angle, close to zero, must be considered [see Fig. 2(c)]. By rotating the BS at this angle, the portion of the transmitted laser beam comes out without deviation. Meanwhile, the reflected portion tilts 2α in such a way that the resulting fringe spacing reduces to $D = \lambda/4\sin(\alpha/2)$ with λ as the wavelength. With this a SCBS is not possible to build an in-line schema due to the optical quality of the cube BS surfaces, typically between $\lambda/4$ and $\lambda/10$, corresponding a distortion the wavefront of between λ and $\lambda/4$, respectively (provided by manufacturer) [27]. An imperfect parallelism of the cube, which implies the beam deviation and, consequently, the slightly off-axis configuration, is depicted in Fig. 2(c). However, our proposal is independent of this limitation by allowing the performance of the dual-plane method with the same SCBS.

A CCD sensor first records the two interference patterns at a distance z from the object plane. These two patterns can be written as

$$H_1(x_1, y_1, z, \phi) = |R_1|^2 + |O_1|^2 + R_1^* O_1 + R_1 O_1^*, \quad (1)$$

$$H_1(x_1, y_1, z, \phi + \pi) = |R_1|^2 + |O_1|^2 - R_1^* O_1 - R_1 O_1^*, \quad (2)$$

where the first two elements on the right hand side of Eqs. (1) and (2) are DC terms, and the last ones represent the real and the virtual images, respectively. In Eqs. (1) and (2), the symbol $*$ denotes complex conjugated, ϕ is the phase term, $R_1 = R * \exp(ik[k_x + k_y + \phi])$, and $R_1 = R * \exp(ik[k_x + k_y + \phi + \pi])$. Here, k_x and k_y are components of wave vector $\mathbf{k}$, and $k = 2\pi/\lambda$ is the wave number.

Then, after an arithmetic operation between Eqs. (1) and (2), one has a pattern free of the DC term:

$$H_{F1}(x_1, y_1, z) = \left[\frac{H_1(x_1, y_1, z, \phi) - H_1(x_1, y_1, z, \phi + \pi)}{2}\right] = R_1^* O_1 + R_1 O_1^*. \quad (3)$$

Once again, we take a record of two additional patterns at a distance $z + \Delta z$ from the object plane, and, with the same arithmetic, we obtain one more pattern free of the DC term:

$$H_{F2}(x_2, y_2, z + \Delta z) = \left[\frac{H_2(x_2, y_2, z + \Delta z, \phi) - H_2(x_2, y_2, z + \Delta z, \phi + \pi)}{2}\right] = R_2^* O_2 + R_2 O_2^*. \quad (4)$$

Equations (3) and (4) show that not only a phase shift but also slightly off-axis scheme can be implemented.

The diffraction patterns of the object $O(x_0, y_0)$, $O_1(x, y, z)$, and $O_2(x, y, z + \Delta z)$ in Eqs. (3) and (4), respectively, can be expressed by using the paraxial approximation of the Kirchhoff–Fresnel propagation [28,29]. Such expressions correspond to

$$O_i(x_i, y_i; z_i) = L\{O(x_0, y_0); z_i\} = O(x_0, y_0) \otimes h(x_0, y_0; x_i, y_i; z_i), \quad (5)$$

where $\otimes$ is the convolution operator, and

$$h(x_0, y_0; x_i, y_i; z_i) = \frac{\exp[jkz_i]}{j\lambda z_i} \exp\left[\frac{jk[(x_i - x_0)^2 + (y_i - y_0)^2]}{2z_i}\right] \quad (6)$$

is the impulse response function. z_i is the distance from the image plane, and $L\{O(x_0, y_0); z_i\}$ stands for the Fresnel free space propagation operator over the corresponding distance z and Δz. Thus, by considering the operations,

$$\psi_1(x_1, y_1) = R_D * H_{F1}(x_1, y_1, z_1) = |R|^2 O_1 + R^2 O_1^*,$$
$$\psi_2(x_2, y_2) = R_D * H_{F2}(x_2, y_2, z_2) = |R|^2 O_2 + R^2 O_2^*. \quad (7)$$

We obtain the relations

$$R^2 O_1^*(x_1, y_1) = L\{R^2 O_2^*(x_2, y_2); \Delta z\}, \quad (8)$$

$$|R|^2 O_2(x_2, y_2) = L\{|R|^2 O_1(x_1, y_1); \Delta z\}, \quad (9)$$

and

$$\Delta\psi(x_1, y_1) = \psi_1(x_1, y_1) - L\{\psi_2(x_2, y_2); \Delta z\} = |R|^2 O_1(x_1, y_1) + R^2 O_1^*(x_1, y_1) - L\{|R|^2 O_2(x_2, y_2); \Delta z\} - L\{R^2 O_2^*(x_2, y_2); \Delta z\}. \quad (10)$$

According to the relations in Eqs. (9) and (10), we have

$$\Delta\psi(x_1, y_1) = |R|^2 O_1(x_1, y_1) - L\{|R|^2 O_1(x_1, y_1); 2\Delta z\}. \quad (11)$$

If R is a unit phasor with a zero phase term (plane wave), then the Fourier transform of $\Delta\psi$ in Eq. (11) implies that

$$\Delta\Psi(f_x, f_y) = \Omega_1(f_x, f_y)[1 - \Gamma\{f_x, f_y; 2\Delta z\}],$$
$$\Omega_1(f_x, f_y) = \frac{\Delta\Psi(f_x, f_y)}{[1 - \Gamma\{f_x, f_y; 2\Delta z\}]},$$
$$\Gamma(f_x, f_y; z_i) = \exp(jz_i k) \exp[-j\pi z_i \lambda[(f_x)^2 + (f_y)^2]], \quad (12)$$

where $\Gamma\{f_x, f_y; z_i\}$ is the free space transfer function over the distance of z_i, and $\Omega_1(f_x, f_y)$ is the Fourier transform of the object $O_1(x)_1, y_1$. Therefore, the object wave corresponds to

$$O(x_0, y_0) = \Im^{-1}\left\{\frac{\Omega_1(f_x, f_y)}{\Gamma\{f_x, f_y; z\}}\right\}, \quad (13)$$

where $\Im^{\pm 1}$ denotes the direct or inverse continuous Fourier transform.

In the following section, we are going to show with a computer simulation that our dual-plane method can be performed in a slightly off-axis configuration and, as we previously commented, is not restricted to be performed only as an in-line configuration.

The motivation for using the slightly off-axis scheme is principally because the commercial BS in the SCBS setup presents some misalignment. In that situation with the proposal, the SCBS is not restricted to having a perfect BS. However, we can obtain two π-shifted holograms, each at the exit of a SCBS in one shot. In addition, SCBS is an interferometer that reduces external vibrations and environment fluctuations, as temperature that avoids errors in phase-shifting. It has a simple implementation and a smaller optical setup.

With this method, no on-line schema or object movement is required. Accuracy of the method lies in how close the reference beam is to a plane wave [21,23]. We use the PSDP method to eliminate the DC term. In the next sections, we are going to explain in more detail the implications of the method.

3. SIMULATIONS

The computational simulations presented in this section are meant to test the proposed method. The first restriction of the method lies in the fact that Δz should be close to 0.1 or 0.05 mm in order to avoid numerical errors [21,24] introduced by the factor

$$1 - \Gamma\{f_x, f_y; 2\Delta z\} \quad (14)$$

in Eq. (12). For the case where $\mathrm{Re}\{\Gamma\{f_x, f_y; 2\Delta z\}\} = 1$, and $\mathrm{Im}\{\Gamma\{f_x, f_y; 2\Delta z\}\} = 0$, the term in Eq. (14) yields zero, then the object $O(x_0, y_0)$ results are undefined. So, it is numerically required that

$$[1 - \Gamma\{f_x, f_y; 2\Delta z\}] \neq 0, \quad (15)$$

or, equivalently, that

$$k2\Delta z - \pi\lambda 2\Delta z[f_x^2 + f_y^2] \neq 2\beta\pi \quad (16)$$

for all possible integers β. Now, Eq. (16) implies

$$\Delta z \neq \frac{\beta\lambda}{2 - \lambda^2(f_x^2 + f_y^2)}, \quad (17)$$

which in discrete form is

$$\Delta z \neq \frac{\beta\lambda MN\delta^2}{2MN\delta^2 - \lambda^2(m^2 + n^2)}. \quad (18)$$

Here, M and N are the total number of pixels in the row and column directions, respectively, where and m and n are integers $(-M/2 < m,\ n > N/2)$. We set $M = N = 2048$, and a CCD pixel pitch $= 6.7$ μm, respectively, and $\delta = \Delta\xi = \Delta\eta$ are the sampling intervals at the observation plane of the camera. We have run a simulation to check the Δz values given by Eq. (18). A change in β implies a variation of Δz on its merit figures. Lower integer values of β increase merit figures of the Δz difference. According to Das *et al.* [22], if we take $\beta = 410$, and $\lambda = 632.8$ nm, Δz varies from 0.10922 to 0.10994 mm. Alternatively, if $\beta = 409$, then Δz varies from 0.10896 to 0.10967 mm. As mentioned by Panezai *et al.* [24], if Δz is equal to an integer multiple of λ, the phase at these two planes would theoretically have the same distribution.

To test the proposed method, we use two synthetic complex objects in order to cover the most possibilities of real world objects. The first one consists of three horizontal bars and three vertical bars with a 100% of transmittance in the substrate. This object simulates static discontinuous surfaces samples. The transmission of each bar is of 100%, and the thickness film corresponds to a phase of 0.7π rad with a 60% transmission [Figs. 3(a) and 3(b)]. On the other hand, the film reduces the illumination power transmission 40%. The second one

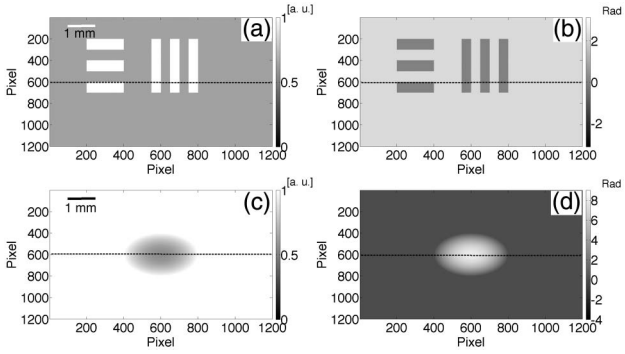

Fig. 3. Objects used in the numerical simulation. (a) Amplitude of a static discontinuous object. (b) Wrapped phase term of the mentioned discontinuous object. (c) Amplitude of a static continuous object. (d) Wrapped phase term of the mentioned continuous object.

consists of a semi-spherical surface deposited in a glass substrate. This object simulates static soft continuous surfaces samples. The size of these objects are 1200×1200 pixels; the distance between the object under test and the CCD plane is $z = 84$ mm. We assumed the working wavelength as $\lambda = 633$ nm (red laser) and a CCD pixel pitch of 6.7 μm (for both, row and column directions).

The recorded object wavefronts were calculated by assuming that the input plane wave is sequentially modulated (in amplitude and phase) by the complex image and propagated along a distance $z = 84$ mm. The resulting wavefronts were then interfered with a plane reference wave of unit amplitude at the camera plane with $\alpha = 200$ μrad in the x and y directions, as Fig. 1 depicts. The holograms were generated according to Eqs. (1) and (2). In the first row of Fig. 4, the holograms of the first object are shown, where (a) and (b) correspond to the shifts 0 and π rad, respectively. These holograms were recorded at the specified distance z. Additional holograms were generated at $z + \Delta z$ with the same shifts, an order of 0 for (c) and π rad for (d). From these four holograms, the proposed method is implemented by using Eqs. (3) and (13). In order to compare the PSDP and SAI with this slightly off-axis configuration, we perform the SAI with two holograms [Figs. 4(a) and 4(c)]. Note that the PSDP and SAI methods remove the DC term. In the second row of Fig. 4, object reconstructions with SAI and PSDP are depicted, where (e) and (g) refer to amplitude distribution, while (f) and (h) correspond to phase distribution, respectively. Figure 4(i) shows an amplitude profile comparison taken along the dashed line in the amplitudes of Figs. 4(e), 4(g), and 3(a). Figure 4(j) shows a phase profile comparison taken along the dashed line in the phases of Figs. 4(f), 4(h), and 3(b). This first simulation result shows that PSDP removes the DC term in a better way than SAI in this off-axis scheme. This observation is present not only in phase distribution but also in the amplitude distribution.

A second simulation test with a soft surface object was performing. In the first row of Fig. 5, we present the generated holograms of the second object, where Fig. 5(a) is 0 rad shifted, and Fig. 5(b) is π rad shifted. These holograms were recorded at a distance of z. Additional holograms were recorded at $z + \Delta z$ with the same shifting order; Fig. 5(c) is 0 rad shifted, and Fig. 5(d) is π rad shifted. Once we have the four holograms, we implement the proposed method; this is from Eqs. (3)–(13). In order to compare the PSDP and SAI with this slightly off-axis configuration, we perform the SAI with two holograms [Figs. 5(a) and 5(c)]. Note that PSDP and SAI methods remove the DC term. In the second row of the Fig. 5 we show the reconstructions of the object, where Figs. 5(e) and 5(g) show the reconstructed amplitude distribution, and Figs 5(f) and 5(h) show the reconstructed phase distribution for the

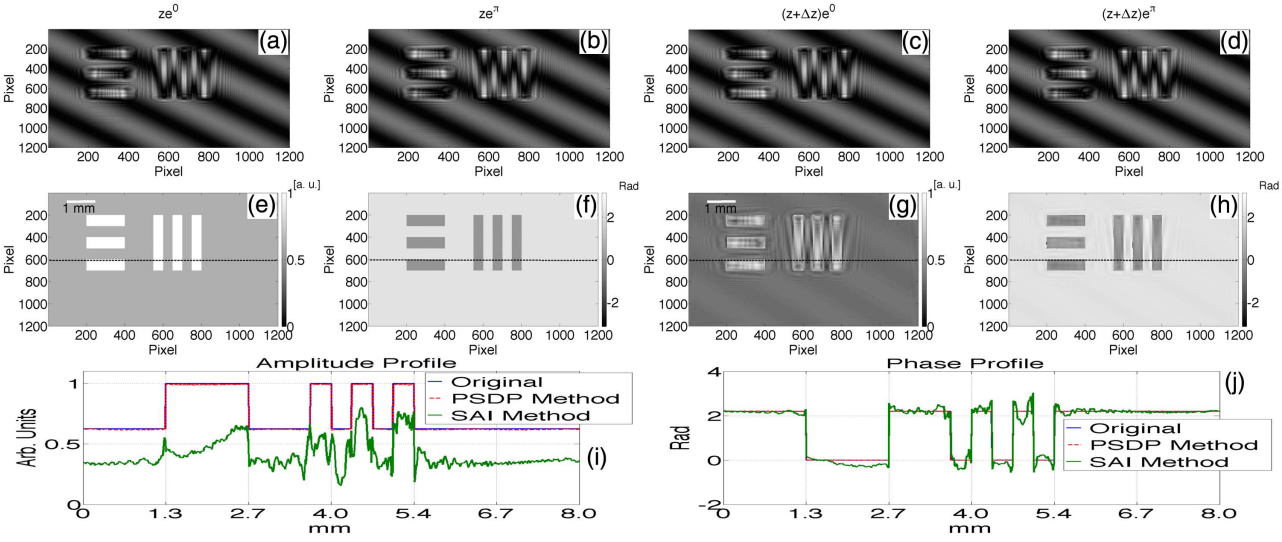

Fig. 4. Simulated amplitude–phase reconstruction of a discontinuous object. (a) and (b) The holograms at distance $z = 84$ mm from the object, zero, and π-shifted, respectively. (c) and (d) The holograms at distance $z = 84.1$ mm from the object, zero, and π–shifted, respectively. (e) and (f) Amplitude and wrapped phase correspondingly derived from the PSDP method. (g) and (h) Amplitude and wrapped phase correspondingly derived from SAI method. (i) Normalized amplitudes along the direction of the dashed line shown in sub-figures (e)–(h) and Fig. 3. (j) Wrapped phase profiles along the aforementioned direction.

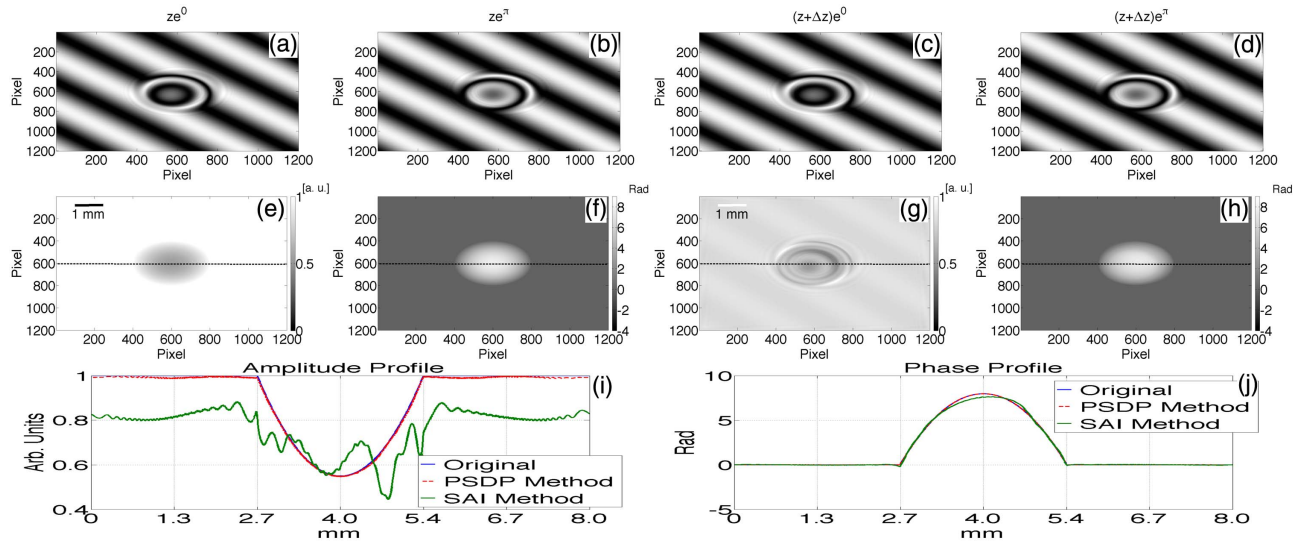

Fig. 5. Simulated amplitude–phase reconstruction of a continuous object. (a) and (b) The holograms at distance $z = 84$ mm from the object, zero, and π-shifted, respectively. (c) and (d) The holograms at distance $z = 84.1$ mm from the object, zero, and π–shifted, respectively. (e) and (f) Amplitude and phase correspondingly derived from the PSDP method. (g) and (h) Amplitude and phase correspondingly derived from the SAI method. (i) Normalized amplitudes along the direction of the dashed line shown in sub-figures (e) and (h) and Fig. 3. (j) Phase profiles along the aforementioned direction.

PSDP and SAI methods, respectively. Figure 5(i) shows an amplitude profile comparison taken along the dashed line in the reconstructed amplitudes of Figs. 5(e), 5(g), and 3(c). Figure 5(j) shows a phase profile comparison taken along the dashed line in the reconstructed phases of Figs. 5(f), 5(h), and 3(d). The same behavior in this second test is present as it in the first one. This second simulation result shows that PSDP removes the DC term in a better way than SAI in this off-axis scheme. This observation is present not only in phase distribution but also in the amplitude distribution. This result confirms that the better method to remove the DC term of Eqs. (1) and (2) is PSDP in the slightly off-axis scheme.

4. RESULTS

In this section, we present the experimental results of the recorded holograms for testing the PSDP proposal with two experiments. In the first one, we used the optical setup shown in Fig. 6 to demonstrate the experimental validation of the proposed PSDP method compared with the well-known standard four-step phase-shifting DH (PSDH) as in Ref. [18] and the SAI method in terms of quantitative accuracy. With this optical setup, all three methods could be straightforwardly tested. In the second experimental test, we used the optical setup shown in Fig. 1 to present the SCBS as an alternative to perform the proposal in two shots. We use a wing bee as the object to be analyzed, and a He–Ne laser ($\lambda = 632.8$ nm) as the illumination source for both experiments. All of the zones of interest are clearly depicted and defined in text and images.

In the first test, two π-shifted holograms were recorded at 77.3 mm from the object [Figs. 7(a) and 7(b)]. Another two π-shifted holograms were recorded at 77.4 mm with respect to the object [Figs. 7(c) and 7(d)]. So, these recordings imply $\Delta z = 0.1$ mm. In our experiments, a black and white complementary metal–oxide–semiconductor (CMOS) camera (8 bits-PixelinkTM PL-B776F) with 1280 × 1024 pixels and a square pixel size of 6.7 μm was used. This camera was coupled on an *xyz*-displacement platform with 10 μm of manual resolution in all directions. The mirror M2 was mounted on a piezoelectric transducer (PZT) to implement the phase-shifting technique.

Figure 8, where each sub-figure column represents a different method, summarizes the first experimental results. Every column represents a different method in the image matrix. Figures 8(a) and 8(d) depict the amplitude and phase distributions, respectively, of the reconstructed object with the PSDH method in the slightly off-axis configuration. Figures 8(b) and 8(e) depict the amplitude and phase distributions, respectively, of the reconstructed object with the PSDP method in the slightly off-axis configuration. Figures 8(c) and 8(f) depict the amplitude and phase distributions, respectively, of the reconstructed object with the SAI method in the slightly off-axis scheme. The third row of Fig. 8 contains the modulus of the amplitude difference between the PSDP and SAI methods versus the PSDH method, respectively. Taking the PSDH method results as a reference (first column), one can note a clear quality difference between the results of the PSDP and SAI methods. Clearly, the PSDP proposal performs best, delivering a complex field that appears almost indistinguishable from the PSDH. The approach using the SAI method, as expected from the previous simulations, returns poor results in quantitative accuracy. The harmonic noise in the PSDP estimations is a consequence of a non-plane reference wave and fringe density. Moreover, simulations with high fringe density offer similar results. On the other hand, a comparison between phase profiles, along a transversal section (dashed line at the middle row) of the bee wing image is performed in Figs. 8(i) and 8(j). It can be seen that the quantitative experimental result of the proposed

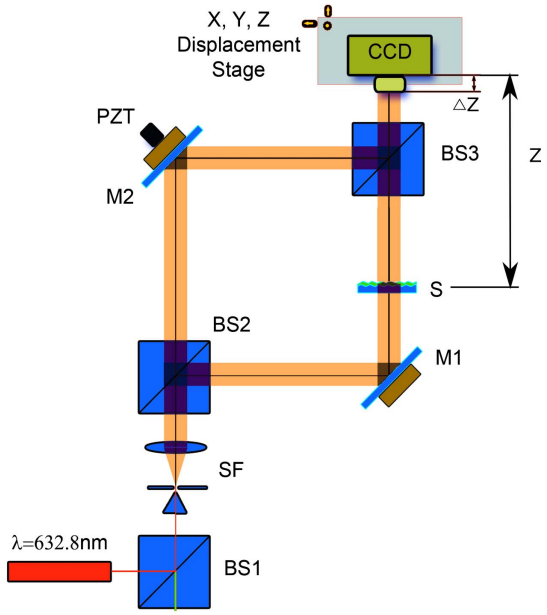

Fig. 6. Experimental setup to perform the PSDP, SAI, and PSDH methods, where SF is a spatial filter and BS is a beam splitter.

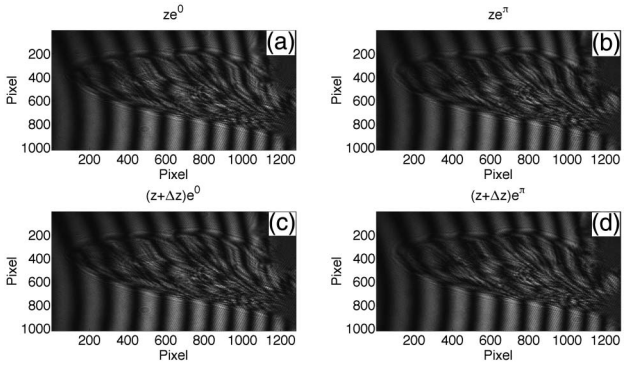

Fig. 7. (a) and (b) Digital holograms π–shifted from each other, recorded at a reconstruction distance of z, and (c) and (d) digital holograms π–shifted from each other, recorded at a reconstruction distance of $z + \Delta z$.

method (PSDP) is in agreement with the standard four-step PSDH result. The slight difference between profiles can be attributed to the phase noise due to the aforementioned fringe density. In addition, a non-plane wave reference [23], laser coherent noise [15], and miscalibration of the PZT encourage this difference in the comparison. Root mean square errors with respect to the PSDH method are provided at the left hand side of items (i) and (j) in Fig. 8. As can be seen, PSDP offers the best result (RMSE = 0.44 rad) at about $\lambda/14$. Although, in this example, the success of the PSDP method seems to be determinant; we need to characterize our method by considering more experimental tests.

In the second test, as we mentioned above, we used the optical setup shown in Fig. 1 to present the SCBS as an alternative to perform the proposal in two shots. We record two holograms at a distance of 10.7 mm from the object to the recording plane.

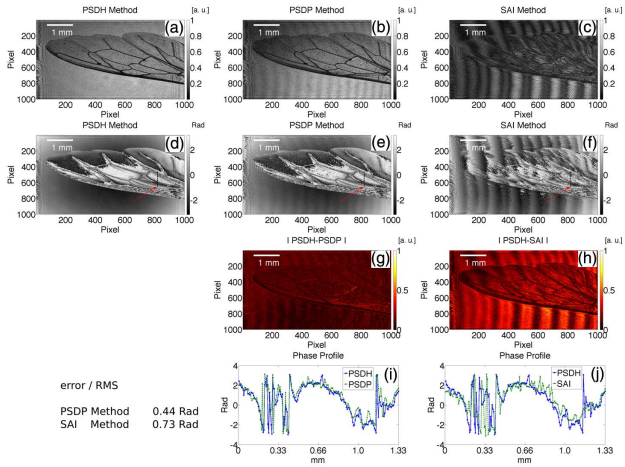

Fig. 8. Experimental comparison of different methods for amplitude and phase holographic reconstructions. The object under investigation is a bee wing. First image column: (a) amplitude and (d) phase reconstruction with the PSDH method that was the reference. Second column: (b) amplitude and (e) phase reconstruction with the PSDP method. Third column: (c) amplitude and (f) phase reconstruction with the SAI method. The third row shows the difference between the PSDH amplitude distribution and (g) PSDP and (h) SAI. The graphs in the fourth row present a comparison between the reconstructed phase distributions.

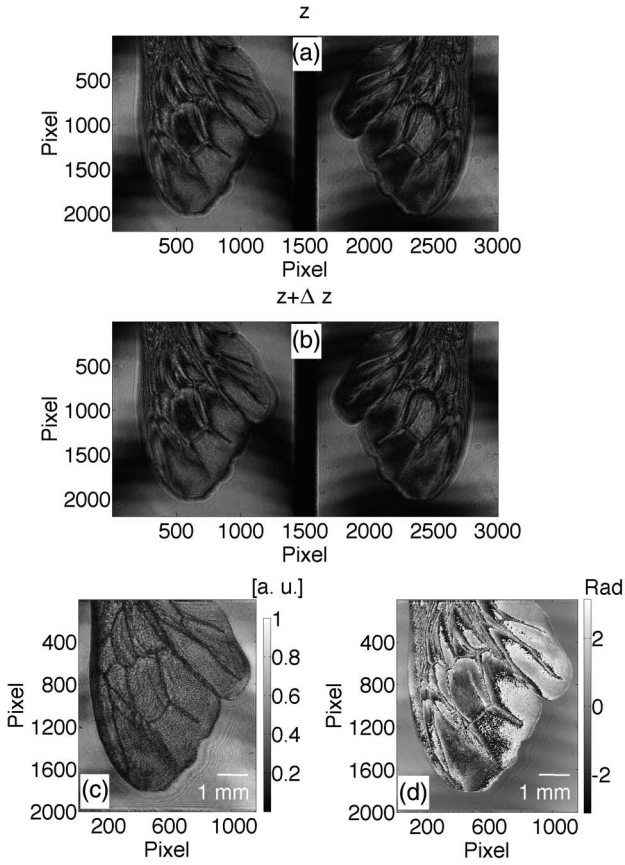

Fig. 9. Digital holograms recorded at (a) the z plane and (b) the $z + \Delta z$ plane. (c) Reconstructed amplitude and (d) wrapped phase images of the sample by using our proposal with SCBS.

With only one shot, we get these holograms π–shifted from each other, as shown Fig. 9(a). A second couple of holograms were recorded at a distance of 10.8 mm from the object to the recording plane; this is depicted in Fig. 9(b). We use a Pixelink CMOS digital camera PL-B781 F. of 3000 × 2208 pixel with a 3.5 μm × 3.5 μm size. Parasitic internal interferences in the SCBS appear. In the interference fringe pattern of Figs. 9(a) and 9(b), one can note this interference because is not a soft curved fringe, it is a slightly wavy fringe. These parasitic interferences can be reduced by using a low coherence illumination source. Figures 9(c) and 9(d) show the amplitude and phase reconstructions, respectively, of the object with the PSDP method in a slightly off-axis configuration. One can note that the quality of the reconstructed distributions is similar to those shown in the preview test. This evaluation suggests that the SCBS is a good alternative to perform the PSDP approach. Some advantages of this SCBS are that only two shots are necessary to perform the proposal. In addition, as SCBS is a compact and monolithic interferometer, insensitivity to external vibrations and environment fluctuations avoids errors in phase-shifting. It is a simple implementation and a smaller optical setup. Our proposal could be applied to monitoring microscopic objects, such as living cells, or alternatively in investigations of non-transparent objects by reflection configurations, as those presented by Asundi *et al.* in Ref. [30].

5. CONCLUSION

We demonstrate a method that significantly improves phase and amplitude distributions in DH based on a dual-plane intensity measurement. The dual-plane method in DH has been performed as an in-line configuration since Zang *et al.* presented it in 2004 [20]. Here, we present that this method also can be performed in a slightly off-axis configuration. The arithmetic procedure, numerical simulations, and experimental results prove the approach and show high accuracy that can be comparable with PSDH. We applied 0 and π phase-shifting in the reference beam to suppress the twin-image and zero-order diffracted wave. A SCBS interferometer is presented to experimentally get the recording of two π-shifted holograms at not only different planes but also when slightly off-axis. The motivation in considering a slightly off-axis schema is principally because a commercial BS in the SCBS presents some misalignment. In such a situation, our proposal is not restricted to working with a perfect BS. However, we can obtain two π-shifted holograms, each at the exit of a SCBS in one shot. In addition, as SCBS is a compact and monolithic interferometer, insensitivity to external vibrations and environmental fluctuations avoids errors in phase-shifting and can automatically compensate phase aberrations. Considering the simplicity and the robustness of this proposal, it represents a valuable tool in many applications. Furthermore, it should be emphasized that the twin image and the DC term are completely removed. This method can be applied in EH in order to get a larger zone of overlap width, lower interference fringe spacing, and a good contrast of the interferometric fringes. In addition, the optical setup can be miniaturized for designing a holographic endoscope.

Funding. Fondo Nacional de Desarrollo Científico y Tecnológico (FONDECYT) (Preis 3140076); Comisión Nacional de Investigación Científica y Tecnológica (CONICYT) (Doctorado Nacional 201363130065).

Acknowledgment. We thank FONDECYT, Act 1410, and UTFSM- DGIP, CONICYT-PCHA/Doctorado Nacional for the support.

REFERENCES

1. J. W. Goodman and R. W. Lawrence, "Digital image formation from electronically detected holograms," Appl. Phys. Lett. **11**, 77–79 (1967).
2. M. A. Kronrod, N. S. Merzlyakov, and P. Yaroslavskii, "Reconstruction of a hologram with a computer," Sov. Phys. Tech. Phys. **17**, 333–334 (1972).
3. U. Schnars and W. Jüptner, "Direct recording of holograms by a CCD-target and numerical reconstruction," Appl. Opt. **33**, 179–181 (1994).
4. V. Kebbel, H. J. Hartmann, and W. Jüptner, "New approach for testing of aspherical micro-optics with high numerical aperture," Proc. SPIE **4451**, 345–355 (2001).
5. M. León-Rodríguez, R. Rodríguez-Vera, J. A. Rayas, and S. Calixto, "Digital holographic microscopy through a Mirau interferometric objective," Opt. Lasers Eng. **51**, 240–245 (2013).
6. F. Charrière, J. Kühn, T. Colomb, F. Monfort, E. Cuche, Y. Emery, K. Weible, P. Marquet, and C. Depeursinge, "Characterization of microlenses by digital holographic microscopy," Appl. Opt. **45**, 829–835 (2006).
7. B. Kemper, S. Stürwald, C. Remmersmann, P. Langehanenbergerg, and G. Von Bally, "Characterization of light emitting diodes (LEDs) for applications in digital holographic microscopy for inspection of micro and nanostructured surfaces," Opt. Eng. **46**, 499–507 (2008).
8. D. Carl, B. Kemper, G. Wernicke, and G. Von Bally, "Parameter optimized digital holographic microscope for high resolution living cells analysis," Appl. Opt. **43**, 6536–6544 (2004).
9. H. Sun, M. Player, J. Watson, D. Hendry, R. Perkins, G. Gust, and D. Paterson, "The uses of digital/electronic holography for biological applications," J. Opt. A **7**, S399–S4007 (2005).
10. B. Rappaz, P. Marquet, E. Cuche, Y. Emery, C. Depeursinge, and P. Magistretti, "Measurement of the integral index and dynamic cell morphometry of living cells with digital holographic microscopy," Opt. Express **13**, 9361–9373 (2005).
11. C. Mann, L. Yu, and M. Kim, "Movies of cellular and sub-cellular motion by digital holographic microscopy," Biomed. Eng. **5**, 21–31 (2006).
12. J. Garcia-Sucerquia, W. Xu, S. K. Jericho, M. H. Jericho, and H. J. Kreuzer, "4-D imaging of fluid flow with digital in-line holographic microscopy," Optik **119**, 419–423 (2008).
13. D. Gabor, "Microscopy by reconstructed wavefronts," Proc. R. Soc. London A **197**, 454–487 (1949).
14. E. N. Leith and J. Upatnieks, "Wavefront reconstruction with defused illumination and three dimensional objects," J. Opt. Soc. Am. **54**, 1295–1301 (1964).
15. M. León-Rodríguez, R. Rodríguez-Vera, J. A. Rayas, and S. Calixto, "High topographical accuracy by optical shot noise reduction in digital holographic microscopy," J. Opt. Soc. Am. A **29**, 498–506 (2012).
16. L. Xu, X. Peng, Z. Guo, J. Miao, and A. Asundi, "Imaging analysis of digital holography," Opt. Express **13**, 2444–2452 (2005).
17. E. Cuche, P. Marquet, and C. Depeursinge, "Simultaneous amplitude-contrast and quantitative phase-contrast microscopy by numerical reconstruction of Fresnel off-axis holograms," Appl. Opt. **38**, 6994–7001 (1999).
18. I. Yamaguchi and T. Zhang, "Phase-shifting digital holography," Opt. Lett. **22**, 1268–1270 (1997).
19. V. Elser, "Phase retrieval by iterated projections," J. Opt. Soc. Am. A **20**, 40–55 (2003).
20. Y. Zang, G. Pedrini, W. Osten, and H. J. Tiziani, "Reconstruction of in-line digital holograms from two intensity measurements," Opt. Lett. **29**, 1787–1789 (2004).

21. G. Situ, J. P. Ryle, U. Gopinathan, and J. T. Sheridan, "Generalized in-line holographic technique based on intensity measurements at two different planes," Appl. Opt. **47**, 711–717 (2008).
22. B. Das, C. S. Yelleswarapu, and D. V. G. L. N. Rao, "Quantitative phase microscopy using dual-plane in-line digital holography," Appl. Opt. **51**, 1387–1395 (2012).
23. J. P. Ryle, D. Li, and J. T. Sheridan, "Dual wavelength digital holographic Laplacian reconstruction," Opt. Lett. **35**, 3018–3020 (2010).
24. S. Panezai, D. Wang, J. Zhao, Y. Wang, and L. Rong, "Dual-plane in-line digital holography based on liquid crystal on silicon spatial light modulator," Appl. Opt. **53**, G105–G110 (2014).
25. J. W. Gates, "Reverse-shearing interferometry," Nature **176**, 359–360 (1955).
26. K. P. Zetie, S. F. Adams, and R. M. Tocknell, "How does a Mach–Zehnder interferometer work?" Phys. Educ. **35**, 46–48 (2000).
27. Thorlabs, https://www.thorlabs.com/newgrouppage9.cfm?objectgroup_id=754.
28. M. Nazarathy and J. Shamir, "Fourier optics described by operator algebra," J. Opt. Soc. Am. **70**, 150–159 (1980).
29. J. W. Goodman, *Introduction to Fourier Optics* (McGraw-Hill, 1996).
30. W. Qu, Z. Wang, C. Y. Cheng, and A. Asundi, "Compound common-path digital holographic microscope," Proc. SPIE **8644**, 864414 (2013).